

Radio Biometrics: Human Recognition Through a Wall

Qinyi Xu, *Student Member, IEEE*, Yan Chen, *Senior Member, IEEE*, BeiBei Wang, *Senior Member, IEEE*, and K. J. Ray Liu, *Fellow, IEEE*

Abstract—In this paper, we show the existence of human radio biometrics and present a human identification system that can discriminate individuals even through the walls in a non-line-of-sight condition. Using commodity Wi-Fi devices, the proposed system captures the channel state information (CSI) and extracts human radio biometric information from Wi-Fi signals using the time-reversal (TR) technique. By leveraging the fact that broadband wireless CSI has a significant number of multipaths, which can be altered by human body interferences, the proposed system can recognize individuals in the TR domain without line-of-sight radio. We built a prototype of the TR human identification system using standard Wi-Fi chipsets with 3×3 multi-in multi-out (MIMO) transmission. The performance of the proposed system is evaluated and validated through multiple experiments. In general, the TR human identification system achieves an accuracy of 98.78% for identifying about a dozen of individuals using a single transmitter and receiver pair. Thanks to the ubiquitousness of Wi-Fi, the proposed system shows the promise for future low-cost low-complexity reliable human identification applications based on radio biometrics.

Index Terms—Human radio biometrics, time-reversal (TR), through-the-wall human identification, radio shot, broadband wireless.

I. INTRODUCTION

NOWADAYS, the capability of performing reliable human identification and recognition has become a crucial requirement in many applications, such as forensics, airport custom check, and bank securities. Current state-of-the-art techniques for human identification rely on the discriminative physiological and behavioral characteristics of human, known as biometrics.

Biometric recognition refers to the automated recognition of individuals based on their human biological and behavioral characteristics [1], [2]. The well-known biometrics for human recognition include fingerprint, face, iris, and voice. Since biometrics are inherent and distinctive to an individual, biometric traits are widely used in surveillance systems for

human identification. Moreover, due to the difficulty for biometrics counterfeiting, techniques based on the biometrics have clear-cut advantages over traditional security methods such as passwords and signatures in countering the growing security threats and in facilitating personalization and convenience. Even though the current biometrics systems are accurate and can be applied in all environments, all of them require special devices that capture human biometric traits in an extremely line-of-sight (LOS) environment, i.e., the subject should make contact with the devices. In this work, a novel concept of radio biometrics is proposed, and accurate human identifications and verifications can be implemented with commercial WiFi devices in a through-the-wall setting.

In [3], researchers studied the relationship between the electromagnetic (EM) absorption of human bodies and the human physical characteristics in the carrier frequency range of 1 to 15 GHz, in which the body's surface area is found to have a dominant effect on absorption. Moreover, the interaction of EM waves with biological tissue was studied [4] and the dielectric properties of biological tissues were measured in [5] and [6]. According to the literature, the wireless propagation around the human body highly depends on the physical characteristic (e.g., height and mass), the total body water volume, the skin condition and other biological tissues. The human-affected wireless signal under attenuations and alterations, containing the identity information, is defined as *human radio biometrics*. Considering the combination of all the physical characteristics and other biological features that affect the propagation of EM waves around the human body and how variable those features can be among different individuals, the chance for two humans to have the identical combinations is significantly small, no matter how similar those features are. Even if two have the same height, weight, clothing and gender, other inherent biological characteristics may be different, resulting in different wireless propagation patterns around the human body. Take the DNA sequence as an example. Even though all humans are 99.5% similar to any other humans, no two humans are genetically identical which is the key to techniques such as genetic fingerprinting [7]. Since the probability of two individuals to have exactly the same physical and biological characteristics is extremely small, the multipath profiles after human interferences are therefore different among different persons. Consequently, human radio biometrics, which record how the wireless signal interacts with a human body, are altered accordingly to individuals' biological and physical characteristics and can be

Manuscript received May 25, 2016; revised October 24, 2016 and November 30, 2016; accepted December 19, 2016. Date of publication January 2, 2017; date of current version February 22, 2017. The associate editor coordinating the review of this manuscript and approving it for publication was Prof. Matti Pietikainen.

Q. Xu, B. Wang, and K. J. R. Liu are with the University of Maryland at College Park, College Park, MD 20742 USA, and also with Origin Wireless, Inc., Greenbelt, MD 20770 USA (e-mail: qinyixu@umd.edu; bebewang@umd.edu; kjrlu@umd.edu).

Y. Chen is with Origin Wireless, Inc., Greenbelt, MD 20770 USA, and also with the University of Electronic Science and Technology of China, Chengdu 611731, China (e-mail: eecyan@uestc.edu.cn).

Color versions of one or more of the figures in this paper are available online at <http://ieeexplore.ieee.org>.

Digital Object Identifier 10.1109/TIFS.2016.2647224

viewed as unique among different individuals. One example is that the face recognition has been implemented for many years to distinguish from and recognize different people, thanks to the fact that different individuals have different facial features. Human radio biometrics, which record how RF signals respond to the entire body of a human including the face, should contain more information than a face, and thus become more distinct among humans. In this work, the proposed TR human identification system utilizes not only the face, but also the entire individual physical characteristic profiles.

In the recent past, a number of attempts have been made to detect and recognize indoor human activities through wireless indoor sensing. Systems have been built to detect indoor human motions based on the variations of CSI [8]–[10]. In [8], the first two largest eigenvalues of the CSI correlation matrix were viewed as features to determine whether the environment is static or dynamic. The standard deviation of the CSI samples from a 3×3 MIMO system combined were fed into SVM to detect human activities such as falling [11]. The received signal strength (RSS) is an indicator for the fluctuation of the wireless channel quality, and thus has been applied to recognize indoor human activities [12]–[15]. Moreover, tracking and recording vital signals using wireless signal has been widely studied [16]–[19]. Liu *et al.* [16] proposed a system to track human breathing and heartbeat rate using off-the-shelf WiFi signals. Vital-Radio system was proposed in [18] that monitors vital signs using radar technique to separate different reflections. On the other hand, the recognition of gestures and small hand motions has been implemented using wireless signals [20]–[23]. Moreover, by sending a specially designed frequency modulated carrier wave (FMCW) which sweeps over different carrier frequencies, Adib and Katabi [24], Adib *et al.* [25]–[27] proposed a new radar-based system to keep track of the different time-of-flights (ToFs) of the reflected signals. However, as focusing on differentiating between different human movements, e. g., standing, walking, falling down and small gestures, none of them have addressed the problem of distinguishing one individual from others, who hold the same posture and stand at the same location, by only using WiFi signals in a through-the-wall setting. Recently, in [27], a RF-Capture system was presented to image human body contour through the wall. Owing to the distinctiveness of silhouettes, it can differentiate between different individuals by applying image processing and machine learning techniques to the captured human figures. However, to get a high-resolution ToF profile, it requires special devices that can scan over 1 GHz spectrum. Moreover, the computational complexity introduced by the necessary image processing and machine learning algorithms is high. On the contrary, this work proposes a novel human identification system that aims at distinguishing and identifying different individuals accurately with commercial MIMO WiFi devices of a 40 MHz transmission bandwidth. The proposed system supports simple and efficient algorithms to achieve a high-accuracy performance.

To achieve this goal, we utilize the time-reversal (TR) technique to capture the differences between human radio biometrics and to reduce the dimension of features. In an indoor environment, there exists a large amount of reflectors

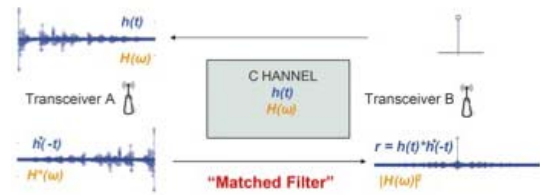


Fig. 1. TR-based wireless transmission.

and scatterers. When a wireless signal emitted from the transmitter encounters them, it will travel along different propagation paths with different distances and suffer different fading effects. Consequently, at the receiver the received signal is a combination of the copies of the same transmitted signal through different paths and delays. This phenomenon is well known as the multipath propagation. TR technique takes advantage of the multipath propagation to produce a spatial-temporal resonance effect. A typical TR wireless communication system is shown in Fig. 1 [28]. Suppose the transceiver A gets an estimated multipath CSI, $\mathbf{h}(t)$, for the channel between A and B, the corresponding TR signature is obtained as $\mathbf{g}(t) = \mathbf{h}^*(-t)$. As the transceiver A transmits back $\mathbf{g}(t)$ over the air, a spatial-temporal resonance is produced at transceiver B. The TR spatial-temporal resonance is generated by fully collecting the energy of the multipath channel and concentrating into a particular location. In physics, the spatial-temporal resonance, which is commonly known as the focusing effect, is the result of a resonance of electromagnetic (EM) field, in response to the environment. This resonance is sensitive to the environment changes, which can be used for capturing the difference in the multipath CSI.

In [29], the concept of TR spatial-temporal resonance has been established as theory and validated through experiments. The TR technique relies on two verified assumptions of channel reciprocity [30], [31] and channel stationarity [28]. Channel reciprocity demonstrates the phenomenon that the CSI of both forward and backward links is highly correlated, whereas channel stationarity establishes that the CSI remains highly correlated during a certain period. A novel TR-based indoor localization approach was first proposed and a prototype was implemented under a 125 MHz bandwidth, achieving a centimeter accuracy even with a single AP working in non-line-of-sight (NLOS) environments [31]. Recently, in [32], a TR indoor locationing system on a WiFi platform was proposed and built, which utilizes the location-specific fingerprints generated by concatenating the CSI with a total equivalent bandwidth of 1 GHz.

In this work, we present a TR human identification system to identify individuals through the walls (i.e., in the absence of any LOS path), based on the human radio biometrics in WiFi signals. To the best of our knowledge, this is the first effort to show and verify the existence of human radio biometrics, which can be found embedding in the wireless channel state information (CSI). Moreover, we propose a human recognition system that extracts the unique radio biometrics as features from the CSI for differentiating between people through the wall. We define the term *radio shot* as the procedure to take

and record human radio biometrics via WiFi signals. The system consists of two main algorithmic parts: the refinement of human radio biometrics and the TR-based identification. The refinement is designed to remove the common CSI components coming from static objects in the environment and the similarity in the radio biometrics of all participants, and to extract the CSI components that contains distinctive human radio biometrics. In the TR-based identification part, the extracted human radio biometric information is mapped into the TR space and the similarity between different biometrics is quantified and evaluated using the time-reversal resonance strength (TRRS). The performance of the proposed identification system is evaluated and the accuracy can achieve a 98.78% identification rate when distinguishing between 11 individuals. The detailed study of performance is in Section V.

The major contributions of this work are summarized below.

- We introduce for the first time the concept of human radio biometrics, which account for the wireless signal attenuation and alteration brought by human. Through experiments, its existence has been verified and its ability for human identification has been illustrated. The procedure to collect human radio biometrics is named as radio shot.
- Due to the fact that the dominant component in the CSI comes from the static environment rather than human body, the human radio biometrics are embedded and buried in the multipath CSI. To boost the identification performance, we design novel algorithms for extracting individual human radio biometrics from the wireless channel information.
- Radio biometrics extracted from the raw CSI are complex-valued and high-dimensional, which complicates the classification problem. To address this problem, we apply the TR technique to fuse and compress the human radio biometrics and to differentiate between radio biometrics of different people, by using the strength of the spatial-temporal resonances.
- For performance evaluation, we build the first prototype that implements the TR human identification system using off-the-shelf WiFi chipsets, and test in an indoor office environment during normal working hours with an identification rate as 98.78% in identifying about a dozen of individuals.

Our work demonstrates the potential of using commercial WiFi signals to capture human radio biometrics for individual identifications.

II. TR HUMAN IDENTIFICATION

The proposed TR human identification system is capable of capturing human biometrics and identifying different individuals through the walls. The human radio biometrics that are embedded in the CSI contain the WiFi reflections and scattering by human body in the indoor environment. As a result, the human radio biometrics, owing to the differences in human biological metrics, are different among different individuals. Moreover, by leveraging the TR technique, in the proposed system, the human radio biometrics can be easily

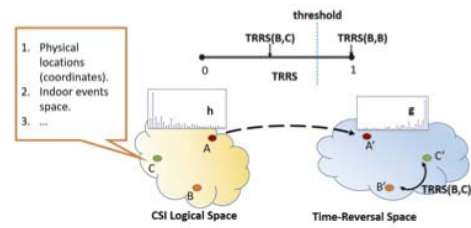


Fig. 2. Mapping between the CSI logical space and the TR space.

extracted from the CSI for distinguishing between individuals. This procedure is called *radio shot*.

A. Time-Reversal Space

During the wireless transmission, signals encounter different objects in the environment, and the corresponding propagation path and characteristics change accordingly before arriving at the receiver. As demonstrated in Fig. 2, each dot in the channel state information (CSI) logical space represents a snapshot of the indoor environment, e.g., an indoor location and an indoor event, which can be uniquely determined by the multipath profile \mathbf{h} . By taking a time-reverse and conjugate operation over the multipath profile, the corresponding TR signature \mathbf{g} is generated. Consequently, each of the points in the CSI logical space as marked by “A”, “B”, and “C” is mapped into the TR space as “A’”, “B’”, and “C’”. In the TR space, the similarity between two profiles is quantified by TRRSs. The higher the TRRS is, the more similar two profiles in the TR space are. Similar profiles constrained by a threshold on TRRS can be treated as a single class. Taking advantage of the TR technique and the TR space, a centimeter-level accurate indoor locationing system was proposed in [31], where each of the indoor physical locations is mapped into a logical location in the TR space and can be easily separated and identified using TRRS. The TR based centimeter-level indoor locationing system was implemented using commercial WiFi chipsets in [32]. By leveraging the TR technique to capture the characteristics of multipath profile at different locations, two locations, even only with a distance of 1 to 2 centimeters, are far away in the TR space and can be easily distinguished.

According to the literature, the wireless propagation around the human body highly depends on the physical characteristic (e.g., height and mass), the total body water volume, the skin condition and other biological tissues. The human radio biometrics, recording the features in interactions between EM waves and human bodies, are unique among different individuals and are mapped into separate points in the TR space. Hence, the proposed system, leveraging the TR technique, is capable of capturing the difference in the multipath profile introduced by different individuals, even when they stand at the same location with the same posture under a through-the-wall setting.

B. The Implementation

The system prototype consists of one 3-antenna transmitter (TX) and one 3-antenna receiver (RX). The CSI samples are obtained from commodity WiFi chips. Moreover,

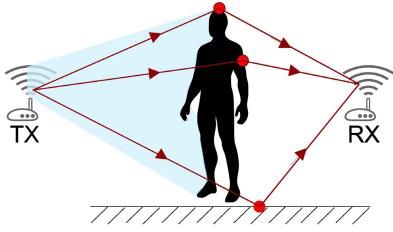


Fig. 3. RF reflections and scattering.

the system is operated at carrier frequency 5.845 GHz with 40 MHz bandwidth. Due to the 3×3 MIMO transmission, each measurement consists of 9 pieces of the CSI for each transmitting-receiving antenna pair. Moreover, for each CSI, it contains 114 complex values representing 114 accessible subcarriers in a 40 MHz band.

To the best of our knowledge, the proposed system is the first that utilizes commodity WiFi signals for human identification.

C. The Challenges

Consider the simplified example in Fig. 3. In an indoor wireless signal propagation environment, the human body acts as a reflector and the red dots represent the reflecting and scattering point due to the human body and other objects. Since the wireless signal reaches the receiving antenna from more than one path, the human radio biometrics are implicitly embedded in the multipath CSI profile. However, the human body may only introduce a few paths to the multipath CSI, and the energy of those paths is small due to the low reflectivity and permittivity, compared with other static objects such as the walls and furniture. As a result, the human radio biometrics, captured through radio shot, are buried by other useless components in the CSI.

Furthermore, due to the fact that the raw CSI obtained from WiFi chips is a 9×114 complex-valued matrix, the resulting raw radio biometrics are of high-dimensional and complex valued, which further complicates the identification and classification problem and increases the computation complexity.

D. The Proposed Solutions

To address the above problems, we exploit the TR techniques and propose several post-processing algorithms to extract the human radio biometrics and magnify the difference among individuals. Specifically, we develop a background subtraction algorithm such that the common information in the CSI can be removed and the distinctive human radio biometrics are preserved. By leveraging the TR technique, the human radio biometrics in the form of complex-valued matrices are related to the corresponding individual through a real-valued scalar, the TRRS.

The design of the proposed time reversal human identification system exploits the above idea and is made up of two key components:

- *Human radio biometrics refinement*: This module extracts the human biometric information from the raw CSI

measurement which is a 9×114 complex-valued matrix. Due to the independency of each link, the background for each link should be calculated and compensated individually. An important consideration is that, for each CSI measurement, it may be corrupted by the sampling frequency offset (SFO) and the symbol timing offset (STO). Hence, before background calculation and compensation, the phase of each CSI measurement should be aligned first. After alignment, based on the assumption that the human radio biometrics only contribute small changes in the multipath, the background can be obtained by taking the average of several CSI measurements.

- *TR-based identification*: Once the 9×114 complex-valued human radio biometric information is refined, this component simplifies the identification problem by reducing the high-dimension complex-valued feature into a real-valued scalar. By leveraging the TR technique, the human radio biometrics are mapped into the TR space and the TRRS quantifies the differences between different radio biometrics. The detailed methodology will be discussed in Section III.

III. SYSTEM MODEL

The proposed system is built upon the fact that the wireless multipath comes from the environment where the EM signals undergo different reflecting and scattering paths and delays. According to the literature, the wireless propagation around the human body highly depends on individual physical characteristics and conditions of biological tissues. Since it is rare for two individuals to have exactly the same biological physical characteristics, the multipath profiles after human interferences are therefore different among different persons. The human radio biometrics, which record how the wireless signal interacts with a human body, is altered accordingly to individuals' biological physical characteristics and can be viewed as unique among different individuals. Through WiFi sounding, the wireless CSI is collected, as well as the human radio biometrics.

Mathematically, the indoor CSI (a.k.a. Channel frequency response, CFR) for the m^{th} link with the presence of human body can be modeled as the sum of the common CSI component and the human affected component:

$$\mathbf{h}_i^{(m)} = \mathbf{h}_0^{(m)} + \delta \mathbf{h}_i^{(m)}, \quad i = 1, 2, \dots, N, \quad (1)$$

where N is the number of individuals to be identified. $\mathbf{h}_i^{(m)}$ is a $L \times 1$ complex-valued vector, which denotes the CSI when the i^{th} individual is inside. L is the number of subcarriers, i.e., the length of the CSI. $\mathbf{h}_0^{(m)}$, defined as the static CSI component, is generated from the static environment in the absence of human, and $\delta \mathbf{h}_i^{(m)}$ denotes the perturbation in the CSI introduced by the i^{th} individual. Here, the $\delta \mathbf{h}_i^{(m)}$ is the raw human radio biometric information of the i^{th} individual embedding in the CSI of the m^{th} link.

At the receiver side, after each channel state sounding, we can collect a $L \times M$ raw CSI matrix for each individual as

$$\mathbf{H}_i = [\mathbf{h}_i^{(1)}, \mathbf{h}_i^{(2)}, \dots, \mathbf{h}_i^{(M)}], \quad \forall i, \quad (2)$$

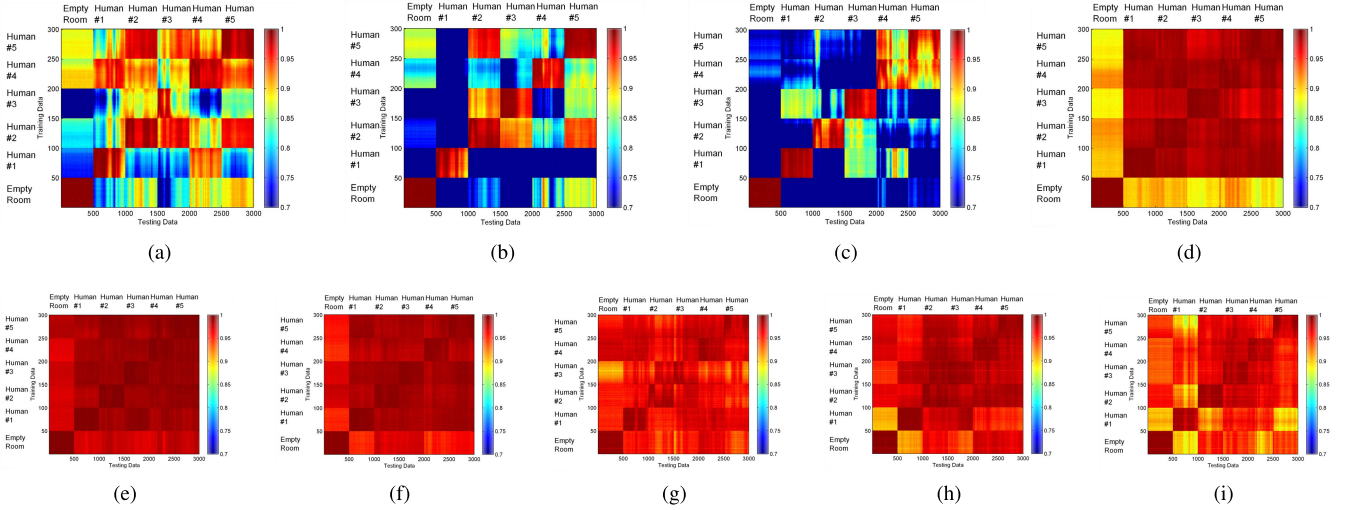


Fig. 4. TRRS map for each link. (a) Link 1. (b) Link 2. (c) Link 3. (d) Link 4. (e) Link 5. (f) Link 6. (g) Link 7. (h) Link 8. (i) Link 9.

with the corresponding human radio biometric information matrix being

$$\delta \mathbf{H}_i = [\delta \mathbf{h}_i^{(1)}, \delta \mathbf{h}_i^{(2)}, \dots, \delta \mathbf{h}_i^{(M)}], \quad \forall i, \quad (3)$$

where M is the number of links between the transmitter and the receiver.

At this point, for human identification and recognition, there are two major problems:

- 1) both $\delta \mathbf{H}_i$ and \mathbf{H}_i are $L \times M$ complex-valued matrix. Without appropriate data processing, the classification problem based on the raw data is complex-valued and of high computation complexity.
- 2) Since we have no idea of what $\mathbf{h}_0^{(m)}$ is, it is hard to extract the buried biometric information $\delta \mathbf{H}_i$ directly from the CSI measurement \mathbf{H}_i .

To tackle the first problem, we incorporate the TR technique to reduce the data dimension by transforming the feature space into TR spatial-temporal resonance as defined in Section III-A. Furthermore, for the second problem, data post-processing algorithms are proposed to refine the human radio biometrics from the raw CSI information as discussed in Section IV.

A. Time-Reversal Spatial-Temporal Resonance

As discussed in Section I, when transmitting back the TR signature through the corresponding multipath channel, a spatial-temporal resonance is generated by fully collecting energy of the multipath channel into a particular location in a rich-scattering indoor environment. The spatial-temporal resonance captures even minor changes in the multipath channel, and it can be utilized to characterize the similarity between two multipath CSI realizations.

The strength of TR spatial-temporal resonance, i.e., the TRRS, in frequency domain is defined as follows.

Definition: The strength of TR spatial-temporal resonance $\mathcal{TR}(\mathbf{h}_1, \mathbf{h}_2)$ in frequency domain between two CFRs

\mathbf{h}_1 and \mathbf{h}_2 is defined as

$$\mathcal{TR}(\mathbf{h}_1, \mathbf{h}_2) = \frac{\max_{\phi} \left| \sum_k \mathbf{h}_1[k] \mathbf{g}_2[k] e^{jk\phi} \right|^2}{\left(\sum_{l=0}^{L-1} |\mathbf{h}_1[l]|^2 \right) \left(\sum_{l=0}^{L-1} |\mathbf{h}_2[l]|^2 \right)}. \quad (4)$$

Here, L is the length of CFR and \mathbf{g}_2 is the TR signature of \mathbf{h}_2 obtained as,

$$\mathbf{g}_2[k] = \mathbf{h}_2^*[k], \quad k = 0, 1, \dots, L-1. \quad (5)$$

Hence, the higher the value of $\mathcal{TR}(\mathbf{h}_1, \mathbf{h}_2)$ is, the more similar are \mathbf{h}_1 and \mathbf{h}_2 .

For two CSI measurements \mathbf{H}_i and \mathbf{H}_j in a MIMO transmission, we can obtain a $1 \times M$ TRRS vector as

$$[\mathcal{TR}(\mathbf{h}_i^{(1)}, \mathbf{h}_j^{(1)}), \mathcal{TR}(\mathbf{h}_i^{(2)}, \mathbf{h}_j^{(2)}), \dots, \mathcal{TR}(\mathbf{h}_i^{(M)}, \mathbf{h}_j^{(M)})].$$

Then, the TRRS between two CSI matrices \mathbf{H}_i and \mathbf{H}_j is defined as the average of the TRRSs on each of the links,

$$\mathcal{TR}(\mathbf{H}_i, \mathbf{H}_j) = \frac{1}{M} \sum_{m=1}^M \mathcal{TR}(\mathbf{h}_i^{(m)}, \mathbf{h}_j^{(m)}). \quad (6)$$

We show an example of the TRRS matrices of each link for different CSI measurements captured by commodity WiFi chips in Fig. 4. Due to the different spatial distributions of each link, how the human body affects the CSI of each link varies. Some link succeeds in capturing the human biometric information and shows distinct TRRSs between different individuals as in Fig. 4c. Whereas, some link fails and the TRRSs between test subjects are similar as shown in Fig. 4e.

B. Identification Methodology

After taking the radio shot, by means of the TR signal processing, the high-dimension complex-valued human radio biometrics embedded in the CSI measurements are mapped into the TR space, and the feature dimension is reduced from $L \times M$ to 1. The human recognition problem can be

implemented as a simple multi-class classification problem as following.

For any CSI measurement \mathbf{H} , given a training database consisting of the CSI samples of each individual \mathbf{H}_i , $\forall i$, the predicted individual identity (ID) is obtained based on the TRRS as:

$$\hat{i} = \begin{cases} \arg \max_i \mathcal{TR}(\mathbf{H}, \mathbf{H}_i), & \text{if } \max_i \mathcal{TR}(\mathbf{H}, \mathbf{H}_i) \geq \mu, \\ 0, & \text{otherwise,} \end{cases} \quad (7)$$

where μ is a predefined threshold for triggering the identification, and $\hat{i} = 0$ denotes an unidentified individual.

However, as discussed above, the embedded human radio biometric information $\delta\mathbf{H}$ is small compared with other CSI components in measurement \mathbf{H} . The resulting TRRS $\mathcal{TR}(\mathbf{H}, \mathbf{H}_i)$ may become quite similar among different samples and thus the accuracy of identification degrades. In order to improve the identification performance, we need to remove the common components from each CSI measurement, and to extract and refine the embedded human biometrics features after taking the radio shot.

IV. RADIO BIOMETRICS REFINEMENT ALGORITHM

As the presence of human body changes the multipath propagation environment of WiFi signals, the human radio biometrics are implicitly embedded in the CSI measurements. However, owing to the fact that only a few paths are affected by the human body, the human biometrics CSI component for the i^{th} individual in the m^{th} link, $\delta\mathbf{h}_i^{(m)}$, is small in energy, compared with the common CSI component $\mathbf{h}_0^{(m)}$ in (1). Without a refinement of the radio biometric information, the common feature $\mathbf{h}_0^{(m)}$ in the CSI dominates in the TRRS in (4) and (6). Moreover, since there exists similarity between different human bodies, it is inevitable to have resemblances in the human radio biometric information $\delta\mathbf{h}_i^{(m)}$. As a result, even though the spatial-temporal resonance captures the $\delta\mathbf{h}_i^{(m)}$, the difference between the TRRSs for different individuals may become too small to differentiate between people. In this work, we propose postprocessing algorithms to extract the useful human radio biometric information from the CSI, after taking the radio shot.

The process of the human radio biometrics refinement includes the following two steps:

- 1) *Phase compensation*: In reality, the estimated CSI can be corrupted by different initial phases of each measurement and different linear phases on each subcarrier due to the time synchronization error. Therefore, in order for the proposed system to extract and subtract out correct background CSI components, it is indispensable to compensate for phase errors in all the raw CSI measurements.
- 2) *Background information subtraction*: Note that the CSI is modeled as the sum of static background CSI components and human biometrics CSI components, so the radio biometric information can be extracted by the system through subtracting out the common information in the CSI.

In what follows, we describe each of the algorithms in detail.

A. Phase Alignment Algorithm

Considering the phase errors, each CSI $\mathbf{h}^{(m)}$ can be mathematically modeled as:

$$\mathbf{h}^{(m)}[k] = \left| \mathbf{h}^{(m)}[k] \right| \exp \left\{ -j(k\phi_{\text{linear}} + \phi_{\text{ini}}) \right\}, \quad k = 0, 1, \dots, L-1, \quad (8)$$

where ϕ_{linear} denotes the slope of the linear phase. ϕ_{ini} is the initial phase, and both of them are different for each CSI.

Unfortunately, there is no way to explicitly estimate either ϕ_{linear} or ϕ_{ini} . To address the phase misalignment among the CSI measurements, for each identification task, we pick one CSI measurement in the training database as the reference and align all the other CSI measurements based on this reference.

To begin with, we find the linear phase difference $\delta\phi_{\text{linear}}$ between the reference and the other CSI samples. For any given CSI \mathbf{h}_2 and reference \mathbf{h}_1 from the same link, we can have

$$\delta\phi_{\text{linear}} = \arg \max_{\phi} \left| \sum_k \mathbf{h}_1[k] \mathbf{h}_2^*[k] \exp \left\{ jk\phi \right\} \right|. \quad (9)$$

To align the linear phase of the CSI \mathbf{h}_2 according to the reference, we simply compensate for this difference on each subcarrier through

$$\hat{\mathbf{h}}_2[k] = \mathbf{h}_2[k] \exp \left\{ -jk\delta\phi_{\text{linear}} \right\}, \quad k = 0, 1, \dots, L-1. \quad (10)$$

Once upon all the linear phase differences of the CSI measurements have been compensated based on the reference, the next step is to cancel the initial phase of the CSI for each link, including the reference. The initial phase is obtained as the phase on the first subcarrier for each CSI $\angle\hat{\mathbf{h}}[0]$, and can be compensated as

$$\mathbf{h}_{\text{align}} = \hat{\mathbf{h}} \exp \left\{ -j\angle\hat{\mathbf{h}}[0] \right\}. \quad (11)$$

In the following discussion, both the background and the refined human biometric information are extracted from the aligned CSI measurements $\mathbf{h}_{\text{align}}$. To simplify notation, we will use \mathbf{h} instead of $\mathbf{h}_{\text{align}}$ to denote the aligned CSI in the rest of the paper.

B. Background Subtraction Algorithm

In the proposed CSI model in (1), the radio biometrics $\delta\mathbf{h}_i^{(m)}$ also involves two parts: the common radio biometric information and the distinct radio biometric information. Thus, $\mathbf{h}_i^{(m)}$ can be further decomposed as following:

$$\mathbf{h}_i^{(m)} = \mathbf{h}_0^{(m)} + \delta\mathbf{h}_{i,c}^{(m)} + \delta\mathbf{h}_{i,d}^{(m)}, \quad \forall i, m, \quad (12)$$

where $\delta\mathbf{h}_i^{(m)} = \delta\mathbf{h}_{i,c}^{(m)} + \delta\mathbf{h}_{i,d}^{(m)}$ denotes the common radio biometric information, which is determined by all the participants in the identification system. Meanwhile, $\delta\mathbf{h}_{i,d}^{(m)}$ is the corresponding distinct radio biometric information,

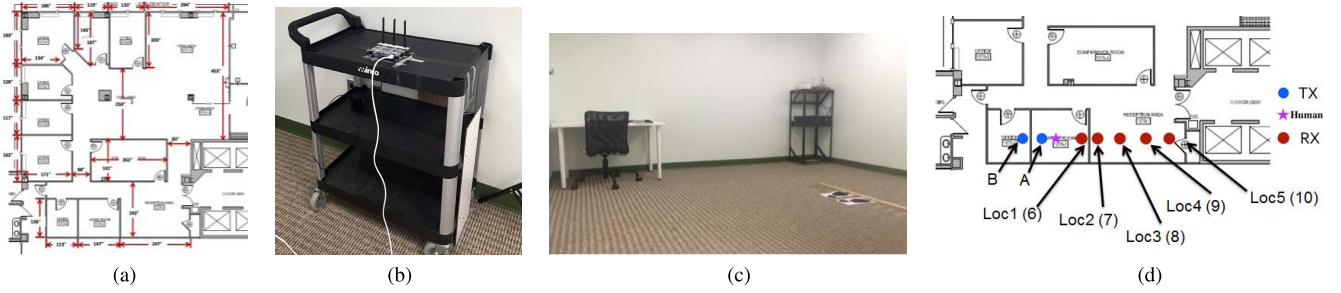


Fig. 5. Experiment setting: floorplan and device. (a) Indoor experiment floorplan with dimensions. (b) Transmitter or receiver devices. (c) Test room configuration. (d) Locations of test subjects and devices.

remaining in the extracted radio biometrics after taking out the common biometric information.

The background CSI components for several CSI measurements of N individuals can be estimated by taking the average over the aligned CSI as:

$$\mathbf{h}_{bg}^{(m)} = \frac{1}{N} \sum_{i=1}^N \frac{\mathbf{h}_i^{(m)}}{\|\mathbf{h}_i^{(m)}\|^2}. \quad (13)$$

Then the human radio biometrics for each individual can be extracted through subtracting a scaled version of the background in (13) from the original CSI.

$$\tilde{\mathbf{h}}_i^{(m)} = \mathbf{h}_i^{(m)} - \alpha \mathbf{h}_{bg}^{(m)}, \quad (14)$$

where α is the background subtraction factor, $0 \leq \alpha \leq 1$. It can not be too close to 1 as the remaining CSI will be noise-like. The impact of α is studied in Section V-B.

After obtaining the refined radio biometrics $\tilde{\mathbf{h}}_i^{(m)}$ for each link, the classification problem based on the TRRS in (7) becomes:

$$\hat{i} = \begin{cases} \arg \max_i \mathcal{TR}(\tilde{\mathbf{H}}, \tilde{\mathbf{H}}_i), & \text{if } \max_i \mathcal{TR}(\tilde{\mathbf{H}}, \tilde{\mathbf{H}}_i) \geq \mu, \\ 0, & \text{otherwise,} \end{cases} \quad (15)$$

where $\tilde{\mathbf{H}}_i$ is the refined radio biometric information matrix for individual i and

$$\tilde{\mathbf{H}}_i = [\tilde{\mathbf{h}}_i^{(1)}, \tilde{\mathbf{h}}_i^{(2)}, \dots, \tilde{\mathbf{h}}_i^{(M)}], \quad \forall i. \quad (16)$$

$\tilde{\mathbf{H}}_i$ is an approximation of the distinctive component in the human radio biometric information matrix $\delta \mathbf{H}_i$ defined in (3).

An example is shown in Fig. 6, where the TRRS $\mathcal{TR}(\mathbf{H}, \mathbf{H}_i)$ before background subtraction is plotted in Fig. 6a while that of $\mathcal{TR}(\tilde{\mathbf{H}}, \tilde{\mathbf{H}}_i)$ is in Fig. 6b, with the background as the average of all CSI measurements in training database. The comparison between two figures demonstrates that the refinement of human radio biometrics helps to improve the sensitivity of TRRS for differentiating between individuals. The proposed background subtraction algorithm suppresses the spatial-temporal resonance of the CSI between different classes while maintaining strong resonance within the same class.

For the proposed system, if there are K subjects to be identified, the computational complexities for building the training database and testing are both $O(M \times (K + 1) \times N \log_2 N)$,

where M is the number of either the training CSI samples or the testing CSI samples for each subject. N is the search resolution for ϕ in (4) and (9), where typical values for N are 512 and 1024.

V. PERFORMANCE EVALUATION

By leveraging the TR technique to capture human radio biometrics embedded in the CSI of WiFi signals, the proposed system is capable of identifying different individuals in real office environments with high accuracy. In this section, the performance of human identification is evaluated. For the proposed system, the training, i.e., taking the radio shot, is simple and can be done in seconds.

A. Experiment Settings

The evaluation experiments are conducted in the office at the 10th floor of a commercial office building with a total of 16 floors. The floorplan of the experiment office is shown in Fig. 5a. Surrounding the experiment office, there are 4 elevators and multiple occupied offices. All the experiments are conducted during the normal working hours in weekdays, so that outside the experiment office there are many activities, such as human walking and elevator running, happening at the same time as the experiments run.

In Fig. 5d the experiment configurations of the transmitter, receiver and individuals are demonstrated. Both WiFi devices are placed on the cart or table with height from the ground being 2.8ft as shown in Fig. 5b. When the transmitter (bot) is on location denoted as ‘‘A’’, the receiver (RX) is placed on the locations denoted from ‘‘Loc 1’’ to ‘‘Loc 5’’. Otherwise when the bot is on location ‘‘B’’, the receiver is on ‘‘Loc 6’’ to ‘‘Loc 10’’ respectively. These 10 TX-RX locations can represent Line-of-sight (LOS) scenario (‘‘Loc 1’’), non LOS (NLOS) scenarios (‘‘Loc 2’’ to ‘‘Loc 6’’), and through-the-wall scenarios (‘‘Loc 7’’ to ‘‘Loc 10’’). When taking the radio shot, each individual, to be recognized, stands in the room on the point marked by the purple star and the door of this room is closed.

Furthermore, in the experiments, we build the training database with 50 CSI measurements for each class, while the size of the testing database for identification is 500 CSI measurements per class. The physical characteristics of test subjects are listed in Table I. The first five subjects participate

TABLE I
PHYSICAL CHARACTERISTICS OF TEST SUBJECTS IN HUMAN IDENTIFICATION EXPERIMENT

Test Subject	#1	#2	#3	#4	#5	#6	#7	#8	#9	#10	#11
Height (cm)	172	164	173	168	176	170	170	172	180	166	155
Weight (kg)	74	53	70	90	90	90	70	69	75	68	45
Gender (M/F)	M	F	M	M	M	M	F	M	M	M	F
Glasses (Y/N)	Y	N	Y	Y	Y	Y	N	Y	Y	Y	N

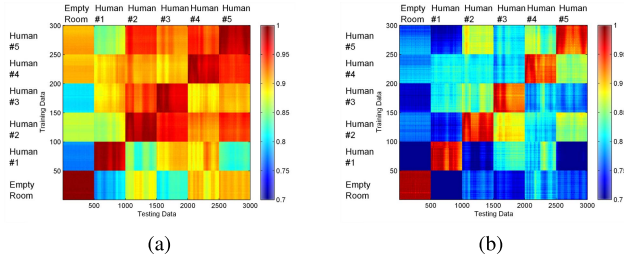


Fig. 6. Comparison on TRRS maps with and without background subtraction. (a) No background subtraction. (b) After background subtraction with $\alpha = 0.5$.

in experiments in Section V-B and Section V-C, while all the 11 subjects take part in the identification experiment in Section V-D. The 2nd individual is the subject in the verification experiments in Section V-E.

B. Impact of Background Subtraction

To begin with, we first quantitatively study the impact of the proposed background subtraction and biometrics refinement algorithms on human recognition.

As shown by Fig. 6, after refinement the spatial-temporal resonance between the training and the testing CSI from different classes is suppressed a lot while maintaining a high TRRS for the CSI from the same class. In Table II, the performance matrices for human identification are listed to show the performance improvement after refining the radio biometrics. Each element of the performance matrix is the probability for that the TRRS between the training and the testing classes is higher than the threshold μ . A higher value in the diagonal means a larger chance of correct identifications. However, larger off-diagonal elements indicate higher false alarm rates because it implies that the testing sample may be misclassified to the wrong training class with a higher probability if the testing class has never been included in the training set.

Both of the matrices in Table II have the same threshold $\mu = 0.9$ as defined in (7) and (15). Without background subtraction, although the diagonal value can reach 100%, the off-diagonal ones can be as high as 99.99% as shown in Table IIa. A high off-diagonal value implies a larger chance to have a false alarm between these particular training and testing classes. Nevertheless, after background subtraction, when using the refined radio biometrics for identification, the largest off-diagonal value drops to 0.24% while maintaining the diagonal elements higher than 96.35%.

TABLE II
PERFORMANCE MATRIX OF INDIVIDUAL IDENTIFICATION WITH AND WITHOUT BACKGROUND SUBTRACTION. (a) NO BACKGROUND SUBTRACTION. (b) AFTER BACKGROUND SUBTRACTION WITH $\alpha = 0.5$.

		Testing Data					
		Empty room	Human #1	Human #2	Human #3	Human #5	
Training Data	Empty room	1	0	0	0	0.4944	0.9613
	Human #5	0	1	0	0.5754	0.4138	0
	Human #4	0	0	1	1	0.9974	1
	Human #2	0	0.3159	1	1	0.1912	0.8869
	Human #3	0.8722	0.4951	0.9917	0.5672	1	1
	Human #1	0.9781	0	1	0.9999	1	1

(a)

(b)

1) *Background Selection*: How to choose the background CSI components is essential for a good radio biometrics refinement. In this part, we study the performance of identification under three schemes: no background subtraction, subtraction with the static environment background, subtraction with the background consisting of static environment and common radio biometrics. We compare the receiver operating characteristic (ROC) curves in Fig. 7a.

The ROC curves, which are obtained by averaging the ROC performance measured at all 10 TX-RX locations, show how the identification rate and false alarm rate vary as the decision threshold μ changes. The red dashed line denotes the performance when using all the CSI measurements in training data set as the background (i.e., the background consisting of static environment and common radio biometrics), while the blue solid line and green dotted line represent the case of no background subtraction and subtraction with the static environment background, respectively. Here, the background subtraction factor is $\alpha = 0.5$. The performance of the system using all the training CSI measurements outperforms the others. The reason is that, by taking the average of the CSI samples from all the classes as the background, we effectively eliminate the high correlated and similar component in radio biometrics for different individuals, which is the estimation of $\mathbf{h}_0^{(m)} + \delta \mathbf{h}_{i,c}^{(m)}$ as defined in (12), and thus enlarge the difference between the radio biometrics of different people.

2) *Optimal Background Subtraction Factor*: After we have determined the optimal background, the next question is to find the optimal background subtraction factor α . In Fig. 7b, the ROC performance is plotted to evaluate the impact of different α . When $\alpha = 0.9$, the identification performance is the worst because the remaining CSI components after background subtraction is noisy and has few information for

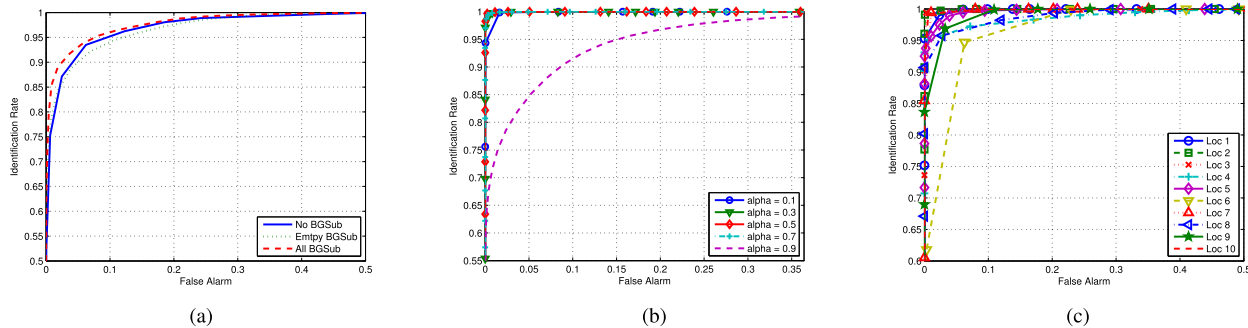


Fig. 7. Evaluation on ROC curves for background subtraction and TX-RX locations. (a) Different selected backgrounds. (b) Different α for Loc 7. (c) Different TX-RX locations.

human biometrics. Through the experiment, we find $\alpha = 0.5$ is optimal for individual identification. In the rest experiments, we adopt $\alpha = 0.5$ and the all-CSI background scheme.

C. Impact of TX-RX Locations

Next, we would like to evaluate the impacts of TX-RX configurations on the performance of human identification. “Loc 1” represents LOS scenario where the transmitter, receiver and experiment individual are in the same room. “Loc 2” to “Loc 6” represent the NLOS case where either the transmitter or the receiver is in the same room with the individual, while the other device is placed outside. Moreover, in the through-the-wall scenarios, represented by “Loc 7” to “Loc 10”, the individual to be identified is in the room while both the transmitter and the receiver are outside and in different locations.

The identification performance of different scenarios is plotted in Fig. 7c. The performance comparison can be summarized from the best to the worst as: Loc 7 > Loc 2 > Loc 3 > Loc 10 > Loc 1 > Loc 5 > Loc 9 > Loc 4 > Loc 8 > Loc 6. There is no direct relation between identification performance and the distance between the transmitter and the receiver. Moreover, the LOS scenario is not the best configuration for human identification. As we discussed, the human radio biometrics are embedded in the multipath CSI. Due to the independency of each paths in the Fr multipath CSI, the more paths the CSI contains, the larger number of degrees of freedom it can provide in the embedded human radio biometrics. Consequently, owing to the fact that there are fewer multipath components in the CSI of the LOS scenario, less informative radio biometrics are extracted, which degrades the performance of identification. The results in Fig. 7c also demonstrate the capability of the proposed system for through-the-wall human identification, in that no matter which configuration is selected the proposed system has a high accuracy.

1) *Special Case Study*: To better understand the impact of TX-RX locations on the identification capability of the proposed system, six examples are investigated and compared in Table III by using the performance matrices defined at the beginning of Section V-B.

In Table IIIa, IIIb and IIIc, the performance matrices for LOS case “Loc 1”, NLOS case “Loc 6” and the through-the-wall case “Loc 7” with the threshold $\mu = 0.9$ are listed. For “Loc 1”, there is no off-diagonal element larger than 0, but the diagonal element for the 5th individual is only 51.59%. This is because in the LOS configuration the human body to be identified is close to both the transmitter and the receiver, which leads to stronger radio biometrics embedded in the CSI. This makes different individuals more distinguishable while making the identification system sensitive and vulnerable to small variations on the human body, e.g., the slight inconsistency in poses and standing location of human. “Loc 6” has the worst performance, since its off-diagonal element could reach 97.32%. Meanwhile, the through-the-wall scenario “Loc 7” becomes the most ideal configuration for individual identification in that the minimum diagonal element is higher than 96% and the largest off-diagonal element is only 0.24%.

Similarly, in Table III d, III e and III f, with the requirement of a minimum diagonal element larger than 99%, the corresponding performance matrices of the aforementioned three cases are shown. To maintain the diagonal values, the identification system has to reduce the threshold μ which inevitably introduces larger off-diagonal elements and more false alarms. Except for the ideal configuration “Loc 7”, the other two examples sacrifice the off-diagonal performance to 91.9% and 99.46% respectively.

We can conclude that among the 10 TX-RX locations tested in the experiment, “Loc 7” is the optimal configuration for the proposed system, and is adopted in the following experiments.

D. Human Identification

From the above analysis, we have already observed that the performance of the proposed human identification system is influenced by both the background subtraction and the TX-RX configurations. In this part, the performance is evaluated in a large data set of 11 individuals, with optimal background subtraction applied and “Loc 7” TX-RX configuration. The corresponding ROC curve is plotted in Fig. 8. With a threshold μ being 0.91, the average identification rate is 98.78% and the average false alarm rate is 9.75%. This is because, when two individuals have similar body contour, the possibility of misclassifying between them increases.

TABLE III

COMPARISON ON PERFORMANCE MATRICES. (a) LOC 1 WITH THRESHOLD $\mu = 0.9$. (b) LOC 6 WITH THRESHOLD $\mu = 0.9$. (c) LOC 7 WITH THRESHOLD $\mu = 0.9$. (d) LOC 1 WITH MINIMUM DIAGONAL > 0.99 . (e) LOC 6 WITH MINIMUM DIAGONAL > 0.99 . (f) LOC 7 WITH MINIMUM DIAGONAL > 0.99

		Testing Data					
		Empty room	Human #1	Human #2	Human #3	Human #4	Human #5
Training Data	Empty room	1	0	0	0	0	0
	Human #1	0	0.9762	0	0	0	0
	Human #2	0	0	0.9887	0	0	0
	Human #3	0	0	0	0.9272	0	0
	Human #4	0	0	0	0	0.9306	0
	Human #5	0	0	0	0	0	0.5159

(a)

		Testing Data					
		Empty room	Human #1	Human #2	Human #3	Human #4	Human #5
Training Data	Empty room	1	0	0	0	0	0
	Human #1	0	0.9896	0	0	0.0912	0
	Human #2	0	0	0.9836	0.8820	0.7128	0.1296
	Human #3	0	0	0.9732	0.9969	0.2052	0.3014
	Human #4	0	0	0.1190	0	1	0.0174
	Human #5	0	0	0.1426	0.3633	0	0.9991

(b)

		Testing Data					
		Empty room	Human #1	Human #2	Human #3	Human #4	Human #5
Training Data	Empty room	1	0	0	0	0	0
	Human #1	0	0.9812	0	0	0	0
	Human #2	0	0	0.9972	0.0024	0	0
	Human #3	0	0	0	0.9635	0	0
	Human #4	0	0	0	0	0.9696	0
	Human #5	0	0	0.0011	0	0	0.9842

(c)

		Testing Data					
		Empty room	Human #1	Human #2	Human #3	Human #4	Human #5
Training Data	Empty room	1	0	0	0	0	0
	Human #1	0	1	0	0	0	0.0430
	Human #2	0	0	1	0.6678	0	0
	Human #3	0	0	0.9190	0.9997	0	0
	Human #4	0	0	0	0.0004	1	0
	Human #5	0	0.1564	0	0	0	0.9977

(d)

		Testing Data					
		Empty room	Human #1	Human #2	Human #3	Human #4	Human #5
Training Data	Empty room	1	0	0	0	0	0
	Human #1	0	0.9972	0	0	0.4843	0
	Human #2	0	0	0.9956	0.9753	0.8852	0.3906
	Human #3	0	0	0.9947	0.9990	0.3744	0.6113
	Human #4	0	0.0110	0.5126	0.0130	1	0.0771
	Human #5	0	0	0.5020	0.6238	0.0048	0.9999

(e)

		Testing Data					
		Empty room	Human #1	Human #2	Human #3	Human #4	Human #5
Training Data	Empty room	1	0	0	0	0	0
	Human #1	0	0.9966	0	0	0	0
	Human #2	0	0	0.9995	0.0443	0	0.0005
	Human #3	0	0	0	0.9905	0	0
	Human #4	0	0	0	0	0.9936	0
	Human #5	0	0	0.0248	0	0	0.9984

(f)

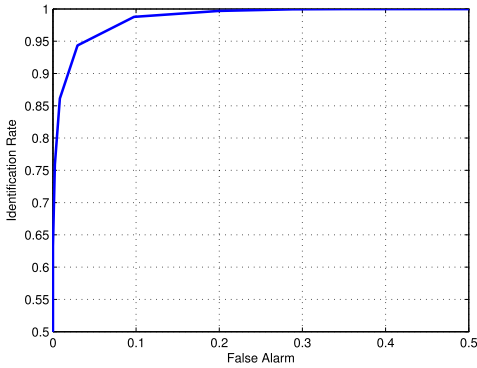


Fig. 8. ROC curve of identifying 11 individuals.

However, since not only the contour but also the permittivity and conductivity of body tissue, which is more distinct for different individuals, will affect the WiFi signal propagation that encounters the human body, the accuracy of identification is still high. In the current performance evaluation, the number of participants is 11. We are inviting more people to participate in the experiment and collecting more data for further validation and analysis.

E. Individual Verification

In this set of experiments, we study the performance of individual verification using proposed system. Instead of finding the correct identity among several possible ones, the individual verification is to recognize a specific individual with variations in both the human body and the environment.

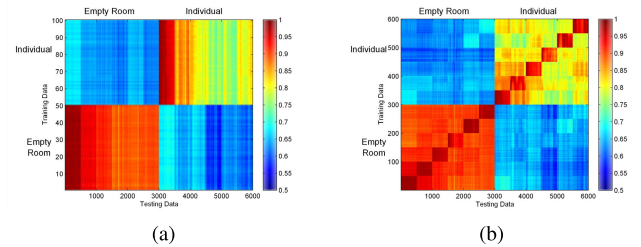


Fig. 9. Comparison on TRRS map on stationarity. (a) No training database updating. (b) With training database updating.

1) *Stationarity Over Time*: To begin with, the stationarity of human verification performance is discussed. We collect the CSI measurements for both the empty room and with one individual inside twice a day for three consecutive days. The TRRS maps are demonstrated in Fig. 9. As shown in Fig. 9a, if we only use the CSI from the first measurement as the training set, the TRRS within the same class gradually decreases. This leads to a 90.83% identification rate with the threshold $\mu = 0.75$. However, if we update the training set every time after measurement and identification, e.g. for Day 2 morning experiment the training set consists of the CSI from measurements at Day 1 morning and afternoon, the identification rate increase to 97.35%. The details of the verification accuracy is listed in Table IV. Hence, to combat the variations over time, the training data set for both identification and verification should be updated regularly.

2) *Other Variations*: In this experiment, the impact of other types of variations such as wearing a coat, carrying a

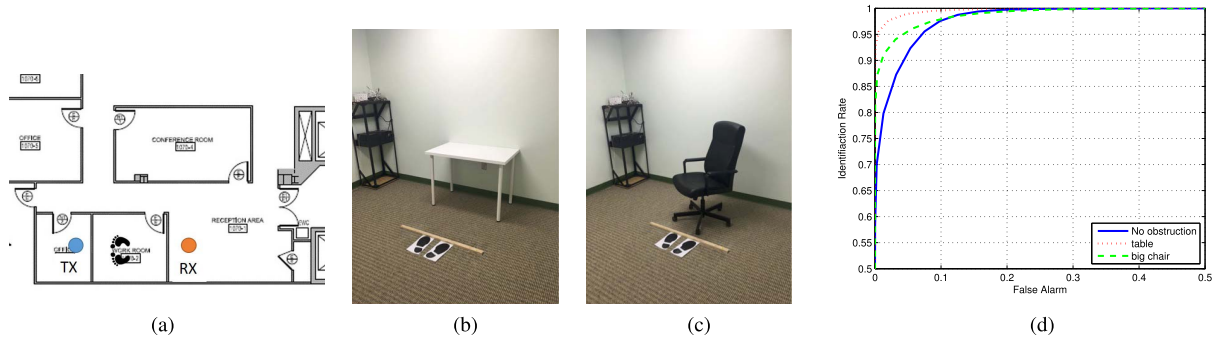


Fig. 10. Evaluation on impacts of obstructions. (a) Test configuration. (b) Behind a table. (c) Behind a chair. (d) ROC curves for different obstructions.

TABLE IV
PERFORMANCE MATRIX FOR STATIONARITY STUDY

		Testing Data					
		Day1-AM	Day1-PM	Day2-AM	Day2-PM	Day3-AM	Day3-PM
Training Data	DAY1-AM	1	1	1	0.8522	0.7400	1
	DAY1-PM	1	1	1	0.9998	0.9856	1
	DAY2-AM	1	0.9989	1	0.9990	0.9997	1
	DAY2-PM	1	0.9926	1	1	0.9999	0.9997
	DAY3-AM	0.8885 8	0.8005	0.9997	0.9833	1	0.9996
	DAY3-PM	1	0.9746	0.9998	0.9420	0.9996	1

TABLE V
LIST OF THE SIX CLASSES OF VARIATION

class	coat	backpack	laptop in the backpack
#1	No	No	No
#2	Yes	No	No
#3	Yes	Yes	No
#4	Yes	Yes	Yes
#5	No	Yes	No
#6	No	Yes	Yes

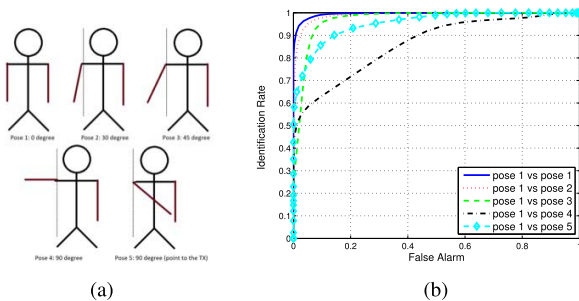


Fig. 11. Study on human pose effects. (a) Test poses. (b) ROC curves with different poses.

backpack/laptop on the accuracy of verification is discussed. We consider six classes as listed in the Table V and the corresponding TRRS map is shown in Fig. 12.

The detailed verification performance is discussed in Table VI where the relation of the threshold μ and the

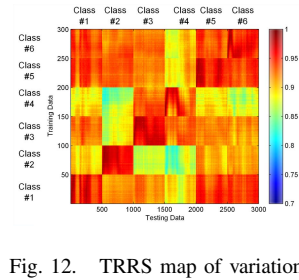


Fig. 12. TRRS map of variation.

TABLE VI
IDENTIFICATION RATE UNDER VARIATIONS

	Threshold 0.92	Threshold 0.9	Threshold 0.85	Threshold 0.84
Class #1	0.9873	0.9994	1	1
Class #2	0.9688	0.9992	1	1
Class #3	0	0.3275	0.9985	1
Class #4	0.4668	0.9756	1	1
Class #5	0.2734	0.9659	1	1
Class #6	0.9720	0.9996	1	1

capability of differentiating between different variations is studied. Here, the training set only contains the CSI from class #1. A low threshold μ reduces the sensitivity of the proposed system in verification. When the threshold μ increases, it may be able to tell whether the individual is wearing a coat and a backpack, shown by the 0 percentage for class #3 to be misclassified as class #1 in Table VI. In terms of the backpack with or without laptop inside, as they are shadowed by the human body, the introduced variations have relatively small impact on the accuracy of verification.

VI. DISCUSSION

Through the above experiments, the capability of identifying and verifying individuals through-the-wall of the proposed TR human identification system has been proved. In this section, the impacts of obstructions and test subjects' postures are evaluated and discussed. The performance of the proposed system is further studied by comparing with a RSSI-based identification system, and the current limitation of the proposed system is discussed.

A. Impacts of Obstructions

Experiments are conducted to evaluate and compare the identification accuracy when there is an obstruction in front

of and in the same room with the test subject. The office configuration is shown in Fig. 10a. The ROC curves for testing under no obstruction, behind a desk as in Fig. 10b and behind a big chair as in Fig. 10c are plotted and compared in Fig. 10d. With a similar level of false alarm, the average identification rate for the no-obstruction scenario is 97.57% and the corresponding average false alarm rate is 9.85%. When there is a table in front of the subject against to the wall, the average identification rate increases to 99.53% while the average false alarm rate is 8.82%. When a big chair is put in front of the test subject with a very short distance, the system has an average identification rate of 97.44% and an average false alarm rate of 8.43%. When there is an obstruction between the test subject and the transceiver, because of the reflections and penetrations, more copies of the transmitted signal are created, along with more multipath components. If the obstruction does not attenuate the signal much, most of the signals radiated from the obstruction will eventually encounter the test subject. Then more radio biometric information can be captured through the multipath propagation, which helps the identification performance. However, if the obstruction is thick in size and has a large vertical surface which attenuates and blocks most of the incoming signals, there will be fewer multipath components passing through the human body. As a result, less informative radio biometrics are obtained, compared with the no-obstruction case. Furthermore, as demonstrated in this experiment, the existence of furniture as the obstruction does not affect the system much.

However, the multipath profile changes when the obstruction changes, especially when the obstruction locates between the transmitter and the receiver link and in front of the test subject. The TR technique is trying to capture the difference in multipath profile, and of course it will capture the difference introduced by obstruction changes in the meantime. Hence, if an individual is behind a large desk during the training phase and later stands behind a small desk for the testing, the proposed system will notice this change in multipath profiles, leading to a mismatch in the training database.

B. Impacts of Human Postures

Experiments have been conducted to evaluate the effects introduced by human poses. Under the setting in Fig. 10a, 4 participants are asked to stand at the same location and perform 5 different poses by lifting their arms with different degrees and directions, as shown in Fig. 11a. The corresponding ROC curves are shown in Fig. 11b.

In the experiment, we select 50 samples for each subject under the 1st pose as the training set. When the testing samples come from the same pose, the identification rate reaches 97.67% with a false alarm rate being 5.58%. However, as the participants change their poses from the 2nd one to the 5th one, the identification rate drops from 95.66% to 88.06%, 58.83% and 79.29% with a false alarm rate around 5.6%. The experimental results validate that pose changes will degrade the system performance. The system is robust to slight changes in posture, e.g., from pose 1 to pose 2. However, as shown by the ROC curve of testing over pose 4 data

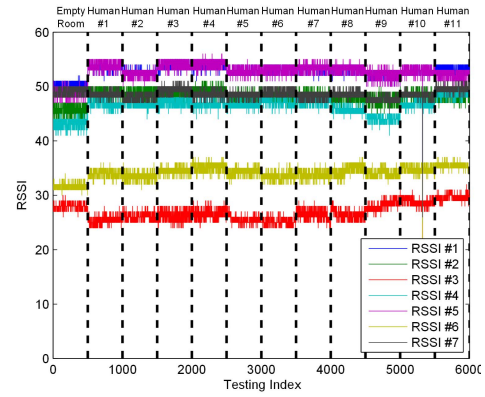


Fig. 13. RSSI values variation of 11 individuals.

with the pose 1 training in Fig. 11b, when the pose alters the propagation environment a lot, the proposed TR human identification system fails to find a match in the training database. In the 4th pose, the test subject is asked to lift the left arm with 90 degree and the direction being perpendicular to the link between the transmitter and the receiver. On the other hand, in the 5th pose, test subjects lift the arm at the same height but the arm is parallel to the TX-RX link. Compared the result of testing over the 5th pose with that over the 4th pose, it is noticed that the identification accuracy drops more if the pose changes the silhouettes in a manner that is perpendicular to the TX-RX link.

Hence, when poses or standing locations change, the multipath profiles in the TR space for a test subjects might fall out of the “proximity” (range of a high similarity) of his or her self, which results in a reduce in the identification rate. Moreover, a worse situation is that the changed multipath profiles fall into the “proximity” of other test subjects which leads to an increase in the false alarm rate.

C. Comparison With RSSI-Based Approach

Using the standard WiFi chipsets, besides the CSI, in each measurement we can also obtain a 7×1 RSS vectors, consisting of 6 RSS values for 3 receiving antenna in each 20 MHz band and 1 overall RSS value. Here, we treat each real-valued 7×1 vector as the feature and apply the k nearest neighbors (kNN) classifiers to the measurements.

1) *RSSI for Identification*: We first test the identification accuracy of the RSSI-based approach on the dataset of 11 individuals. From the results in Fig. 13, the RSSI difference between different individuals is small. The false alarm rate is 68.07% and the identification rate is only 31.93%, which is far inferior to the proposed identification system.

2) *RSSI for Verification*: In Fig. 14, the stationarity is evaluated and from the plot it is obvious that the RSS value is not stable over time. Without training database update, the identification rate for the individual is only 89.67% with a 10.33% possibility that the individual is misclassified as an empty room. Even with the training database update, the identification rate does not improve due to the instability of the RSS values over time.

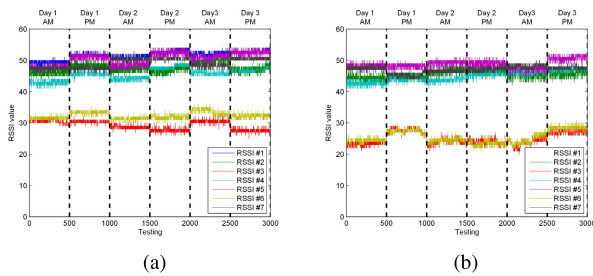


Fig. 14. RSSI values comparison on stationarity. (a) RSSI for empty room. (b) RSSI with individual present.

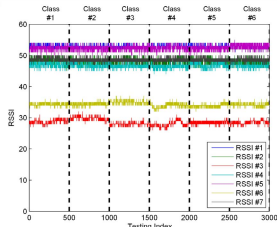


Fig. 15. RSSI values comparison on variations.

TABLE VII
CONFUSION MATRIX UNDER RSSI-BASED APPROACH

		Testing Data					
		Class #1	Class #2	Class #3	Class #4	Class #5	Class #6
Training Data	Class #1	0.3140	0.3680	0.0840	0.0840	0.1980	0.2260
	Class #2	0.0220	0.0280	0.0020	0	0.0420	0.0040
	Class #3	0.0540	0.0840	0.2920	0.1360	0.0660	0.0980
	Class #4	0.2340	0.0220	0.4600	0.4360	0.2940	0.2600
	Class #5	0.1040	0.1160	0.0100	0.1020	0.1260	0.0740
	Class #6	0.2620	0.3820	0.1520	0.2420	0.2740	0.3380

Furthermore, in terms of verifying individual with small variations as listed in Table VI, the RSSI-based approach can hardly differentiate between different variations by only using the 7×1 RSS vector as shown in Fig. 15 and in the confusion matrix of individual verification in Table VII. The reason for its insensitivity to small variations is the same as that for its incapability in human identification. The 7×1 RSS vector feature only captures little human radio biometric information and loses the individual discrimination.

Hence, even though the RSSI-based approach is robust to the small variations on human body, it cannot be put into practice for human identification and verification. Moreover, since RSSI is only a real-valued scaler which approximately represents the received signal power, it is less informative, susceptible to noise and has large intra-class variations which degrades the identification accuracy a lot when the number of test subjects increases. Compared with the RSSI-based approach, the proposed TR human identification system succeeds in capturing and extracting the human radio biometric information embedded in the CSI, and in distinguishing individuals with high accuracy through-the-wall.

D. Limitations

At current stage, the proposed TR human identification system exhibits some limitations:

- 1) The proposed system adopts a simple model for human radio biometrics embedded in the CSI as shown in (1). As a result, the obtained human radio biometrics $\delta\mathbf{h}$ and the environment component \mathbf{h}_0 is correlated. In other words, the human radio biometrics $\delta\mathbf{h}$ is location-dependent, which requires the system to run in an environment consistent over time. Future work includes developing algorithms to separate the human radio biometrics and the outside environment.
- 2) Current system is equipped with only one pair of the transmitter and the receiver, and hence its performance can be improved by deploying more transceiver pairs to capture fine-grained human radio biometrics from different directions simultaneously.
- 3) In the current work, it is difficult to scientifically prove the uniqueness of human radio biometrics, when taking into account how complicated the techniques it requires to extract all of these biological features from each individual are. In the future work, experiments that involve more subjects will be conducted and techniques that can record other biological features will be utilized to provide more details in human biological characteristics, such as the muscle mass index and the body temperature. With more detailed information regarding individual biological features besides the common information like height, weight, gender and clothing, the uniqueness of radio biometrics can be well studied, tested and verified.

Despite these limitations, we believe the proposed TR human identification system should be viewed as a milestone in the development of both the human identification systems and wireless sensing systems. For the current system, it can be implemented in the environments that remain stationary most of the time. For example, it can be implemented for identity verification at places like bank vaults to allow the entry of authorized staff. It can also be used in home security systems, functioning as wireless electronic keys in vacation houses. Moreover, the location embedded radio biometrics are helpful in applications that require to tell both who the test subject is and where the test subject is. Once the environment-independent radio biometric information is extracted out, the proposed system can work to identify individuals without noticed by test subjects and implement in applications that require no direct contact with test subjects or where there are obstructions in-between the sensor and the subject.

VII. CONCLUSIONS

We propose a TR human identification system, where individuals are distinguished from and identified by the human radio biometrics extracted from the WiFi CSI through the TR technique. Furthermore, the existence of the human radio biometrics, which can be found embedding in the indoor WiFi signal propagation and captured through radio shot, is shown and verified in this work. As this new type of biometrics is introduced, it motivates a novel human identification technique relying on wireless sensing with WiFi signals. By leveraging the TR technique to extract radio biometrics, a low-complexity human identification system can be widely

implemented without restrictions on the device deployment thanks to the ubiquitousness of WiFi.

REFERENCES

- [1] A. Jain, A. A. Ross, and K. Nandakumar, *Introduction to Biometrics*. Springer, 2011.
- [2] A. K. Jain, K. Nandakumar, and A. Ross, "50 years of biometric research: Accomplishments, challenges, and opportunities," *Pattern Recognit. Lett.*, vol. 79, pp. 80–105, Aug. 2016.
- [3] G. Melia, *Electromagnetic Absorption by the Human Body From 1-15 GHz*. York, U.K.: Univ. York, 2013.
- [4] P. Beckmann and A. Spizzichino, *The Scattering of Electromagnetic Waves From Rough Surfaces*. Norwood, MA, USA: Artech House, 1987.
- [5] S. Gabriel, R. W. Lau, and C. Gabriel, "The dielectric properties of biological tissues: II. Measurements in the frequency range 10 Hz to 20 GHz," *Phys. Med. Biol.*, vol. 41, no. 11, p. 2251, 1996.
- [6] S. Gabriel, R. W. Lau, and C. Gabriel, "The dielectric properties of biological tissues: III. Parametric models for the dielectric spectrum of tissues," *Phys. Med. Biol.*, vol. 41, no. 11, p. 2271, 1996.
- [7] S. Levy *et al.*, "The diploid genome sequence of an individual human," *PLoS Biol.*, vol. 5, no. 10, p. e254, 2007.
- [8] J. Xiao, K. Wu, Y. Yi, L. Wang, and L. M. Ni, "FIMD: Fine-grained device-free motion detection," in *Proc. IEEE 18th Int. Conf. Parallel Distrib. Syst. (ICPADS)*, Dec. 2012, pp. 229–235.
- [9] W. Wang, A. X. Liu, M. Shahzad, K. Ling, and S. Lu, "Understanding and modeling of WiFi signal based human activity recognition," in *Proc. 21st Annu. Int. Conf. Mobile Comput. Netw.*, 2015, pp. 65–76.
- [10] W. Xi *et al.*, "Electronic frog eye: Counting crowd using WiFi," in *Proc. Int. Conf. Comput. Commun.*, Apr. 2014, pp. 361–369.
- [11] C. Han, K. Wu, Y. Wang, and L. Ni, "Wifall: Device-free fall detection by wireless networks," in *Proc. Int. Conf. Comput. Commun.*, Apr. 2014, pp. 271–279.
- [12] C. R. R. Sen Souvik and N. Srihari, "Spinloc: Spin once to know your location," in *Proc. 12th Workshop Mobile Comput. Syst. Appl. HotMobile*, New York, NY, USA, 2012, pp. 12:1–12:6.
- [13] S. Sigg, S. Shi, F. Buesching, Y. Ji, and L. Wolf, "Leveraging RF-channel fluctuation for activity recognition: Active and passive systems, continuous and RSSI-based signal features," in *Proc. Int. Conf. Adv. Mobile Comput. Multimedia (MoMM)*, New York, NY, USA, 2013, pp. 43:43–43:52.
- [14] A. Banerjee, D. Maas, M. Bocca, N. Patwari, and S. Kasera, "Violating privacy through walls by passive monitoring of radio windows," in *Proc. ACM Conf. Secur. Privacy Wireless Mobile Netw. (WiSec)*, New York, NY, USA, 2014, pp. 69–80.
- [15] H. Abdelnasser, K. Harras, and M. Youssef, "WiGest demo: A ubiquitous WiFi-based gesture recognition system," in *Proc. Int. Conf. Comput. Commun. Workshops*, Apr. 2015, pp. 17–18.
- [16] J. Liu, Y. Wang, Y. Chen, J. Yang, X. Chen, and J. Cheng, "Tracking vital signs during sleep leveraging off-the-shelf WiFi," in *Proc. 16th ACM Int. Symp. Mobile Ad Hoc Netw. Comput. MobiHoc*, New York, NY, USA, 2015, pp. 267–276.
- [17] H. Abdelnasser, K. A. Harras, and M. Youssef, "UbiBreathe: A ubiquitous non-invasive WiFi-based breathing estimator," in *Proc. 16th Int. Symp. Mobile Ad Hoc Netw. Comput. MobiHoc*, New York, NY, USA, 2015, pp. 277–286.
- [18] F. Adib, H. Mao, Z. Kabelac, D. Katabi, and R. C. Miller, "Smart homes that monitor breathing and heart rate," in *Proc. 33rd Annu. ACM Conf. Human Factors Comput. Syst. CHI*, New York, NY, USA, 2015, pp. 837–846.
- [19] R. Ravichandran, E. Saba, K. Y. Chen, M. Goel, S. Gupta, and S. N. Patel, "WiBreathe: Estimating respiration rate using wireless signals in natural settings in the home," in *Proc. Int. Conf. Pervasive Comput. Commun.*, Mar. 2015, pp. 131–139.
- [20] Q. Pu, S. Gupta, S. Gollakota, and S. Patel, "Whole-home gesture recognition using wireless signals," in *Proc. 19th Annu. Int. Conf. Mobile Comput. Netw.*, 2013, pp. 27–38.
- [21] H. Abdelnasser, M. Youssef, and K. A. Harras, "WiGest: A ubiquitous WiFi-based gesture recognition system," in *Proc. Int. Conf. Comput. Commun.*, May 2015, pp. 1472–1480.
- [22] L. Sun, S. Sen, D. Koutsonikolas, and K.-H. Kim, "WiDraw: Enabling hands-free drawing in the air on commodity WiFi devices," in *Proc. 21st Annu. Int. Conf. Mobile Comput. Netw.*, 2015, pp. 77–89.
- [23] K. Ali, A. X. Liu, W. Wang, and M. Shahzad, "Keystroke recognition using WiFi signals," in *Proc. 21st Annu. Int. Conf. Mobile Comput. Netw.*, 2015, pp. 90–102.
- [24] F. Adib and D. Katabi, "See through walls with WiFi!" in *Proc. ACM SIGCOMM Conf.*, New York, NY, USA, 2013, pp. 75–86.
- [25] F. Adib, Z. Kabelac, D. Katabi, and R. C. Miller, "3D tracking via body radio reflections," in *Proc. 11th USENIX Symp. Netw. Syst. Design Implement.*, Seattle, WA, USA, Apr. 2014, pp. 317–329.
- [26] F. Adib, Z. Kabelac, and D. Katabi, "Multi-person localization via RF body reflections," in *Proc. 12th USENIX Symp. Netw. Syst. Design Implement.*, Oakland, CA, USA, May 2015, pp. 279–292.
- [27] F. Adib, C.-Y. Hsu, H. Mao, D. Katabi, and F. Durand, "Capturing the human figure through a wall," *ACM Trans. Graph.*, vol. 34, no. 6, pp. 219:1–219:13, Oct. 2015.
- [28] B. Wang, Y. Wu, F. Han, Y.-H. Yang, and K. J. R. Liu, "Green wireless communications: A time-reversal paradigm," *IEEE J. Sel. Areas Commun.*, vol. 29, no. 8, pp. 1698–1710, Sep. 2011.
- [29] J. de Rosny, G. Lerosey, and M. Fink, "Theory of electromagnetic time-reversal mirrors," *IEEE Trans. Antennas Propag.*, vol. 58, no. 10, pp. 3139–3149, Oct. 2010.
- [30] G. Lerosey, J. de Rosny, A. Tourin, A. Derode, G. Montaldo, and M. Fink, "Time reversal of electromagnetic waves," *Phys. Rev. Lett.*, vol. 92, no. 19, p. 193904, 2004.
- [31] Z.-H. Wu, Y. Han, Y. Chen, and K. J. R. Liu, "A time-reversal paradigm for indoor positioning system," *IEEE Trans. Veh. Technol.*, vol. 64, no. 4, pp. 1331–1339, Apr. 2015.
- [32] C. Chen, Y. Chen, K. J. R. Liu, Y. Han, and H.-Q. Lai, "High accuracy indoor localization: A WiFi-based approach," in *Proc. IEEE Int. Conf. Acoust. Speech Signal Process. (ICASSP)*, Mar. 2016, pp. 6245–6249.



Qinyi Xu (S'15) received the B.S. degree (Highest Hons.) in information engineering from Southeast University, Nanjing, China, in 2013. She is currently pursuing the Ph.D. degree with the Department of Electrical and Computer Engineering, University of Maryland at College Park, College Park, MD, USA. Her current research interests include signal processing and wireless communications.

Miss Xu is a recipient of the Clark School Distinguished Graduate Fellowships from the University of Maryland at College Park, and the Graduate with Honor Award from Southeast University in 2013. She was an Exchange Student with the KTH-Royal Institute of Technology, Stockholm, Sweden, from 2012 to 2013, with the national sponsorship of China.



Yan Chen (SM'14) received the bachelor's degree from the University of Science and Technology of China in 2004, the M.Phil. degree from the Hong Kong University of Science and Technology in 2007, and the Ph.D. degree from the University of Maryland at College Park, College Park, MD, USA, in 2011. Being a Founding Member, he joined Origin Wireless Inc. as a Principal Technologist in 2013. He is currently a Professor with the University of Electronic Science and Technology of China. His research interests include multimedia, signal processing, game theory, and wireless communications.

Dr. Chen is a recipient of multiple honors and awards, including the Best Student Paper Award at IEEE ICASSP in 2016, the best paper award at IEEE GLOBECOM in 2013, the Future Faculty Fellowship and Distinguished Dissertation Fellowship Honorable Mention from the Department of Electrical and Computer Engineering in 2010 and 2011, the Finalist of the Dean's Doctoral Research Award from the A. James Clark School of Engineering, the University of Maryland at College Park in 2011, and the Chinese Government Award for outstanding students abroad in 2010.



Beibei Wang (SM'15) received the B.S. degree (Highest Hons.) in electrical engineering from the University of Science and Technology of China, Hefei, in 2004, and the Ph.D. degree in electrical engineering from the University of Maryland at College Park, in 2009. She was with the University of Maryland as a Research Associate from 2009 to 2010, and with Qualcomm Research and Development from 2010 to 2014. Since 2015, she has been with Origin Wireless Inc., as a Principle Technologist. Her research interests include wireless

communications and signal processing. She received the Graduate School Fellowship, the Future Faculty Fellowship, the Dean's Doctoral Research Award from the University of Maryland, and the Overview Paper Award from the IEEE Signal Processing Society in 2015. She is a co-author of *Cognitive Radio Networking and Security: A Game-Theoretic View* (Cambridge University Press, 2010).



K. J. Ray Liu (F'03) was named a Distinguished Scholar-Teacher of the University of Maryland at College Park, College Park, in 2007, where he is Christine Kim Eminent Professor of Information Technology. He leads the Maryland Signals and Information Group conducting research encompassing broad areas of information and communications technology with recent focus on smart radios for smart life.

Dr. Liu was a recipient of the 2016 IEEE Leon K. Kirchmayer Technical Field Award on graduate teaching and mentoring, IEEE Signal Processing Society 2014 Society Award, and IEEE Signal Processing Society 2009 Technical Achievement Award. Recognized by Thomson Reuters as a Highly Cited Researcher, he is a Fellow of AAAS. He is a member of IEEE Board of Directors. He was President of IEEE Signal Processing Society, where he has served as Vice President – Publications and Board of Governor. He has also served as the Editor-in-Chief of *IEEE Signal Processing Magazine*. He also received teaching and research recognitions from University of Maryland including university-level Invention of the Year Award; and college-level Poole and Kent Senior Faculty Teaching Award, Outstanding Faculty Research Award, and Outstanding Faculty Service Award, all from A. James Clark School of Engineering.